Article

Mesoporous Compound Semiconductors from the Reaction of Metal Ions with Deltahedral [Ge] Clusters

Gerasimos S. Armatas, and Mercouri G. Kanatzidis

J. Am. Chem. Soc., **2008**, 130 (34), 11430-11436 • DOI: 10.1021/ja802940w • Publication Date (Web): 05 August 2008

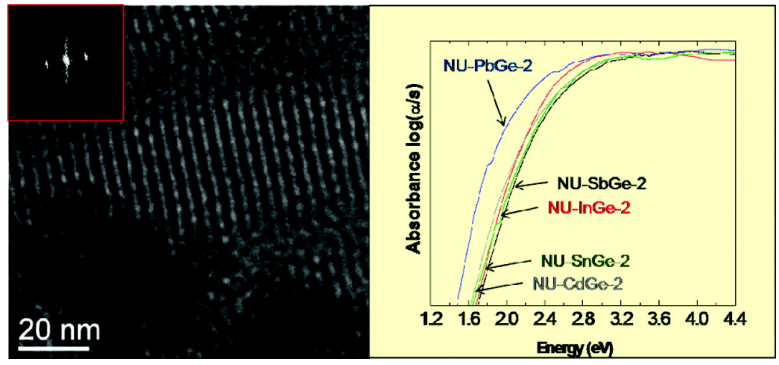

More About This Article

Additional resources and features associated with this article are available within the HTML version:

- Supporting Information
- Access to high resolution figures
- Links to articles and content related to this article
- Copyright permission to reproduce figures and/or text from this article

View the Full Text HTML

J|A|C|S
ARTICLES

Published on Web 08/05/2008

Mesoporous Compound Semiconductors from the Reaction of Metal Ions with Deltahedral $[Ge_9]^{4-}$ Clusters

Gerasimos S. Armatas† and Mercouri G. Kanatzidis*,†,‡

Department of Chemistry, Northwestern University, Evanston, Illinois 60208, and Materials Science Division, Argonne National Laboratory, Chicago, Illinois 60439

Received April 21, 2008; E-mail: m-kanatzidis@northwestern.edu

Abstract: We report the surfactant-directed assembly of mesoporous metal/germanium-based semiconducting materials from coupling of anionic $(Ge_9)^{4-}$ clusters with various linking metal ions. The resulting materials feature a metal/Ge_9 framework perforated by regular arrays of mesoporous channels. The permanent mesoporosity of the materials NU-MGe-2 (M = Sb, In, Sn, Pb, Cd), determined by N_2 physisorption measurements, corresponds to high internal BET surface areas from 127 to 277 m^2/g and total pore volumes from 0.15 to 0.26 cm^3/g. The mesoporous structures exhibit energy gaps in the range of 1.48−1.70 eV as well as strong photoluminescence at room temperature with emission energies varying from 740 to 845 nm. The emission depends on pore wall thickness and framework composition. The photoemission intensity in the mesoporous intermetallic germanium-based frameworks can be selectively suppressed by adsorbing electron-acceptor species such as tetracyanoethylene molecules but remains unchanged when exposed to electron-donor species such as tetrathiafulvalene molecules.

Introduction

Dimensionally reduced semiconductor structures such as nanoparticles and quantum dots are impacting a diverse set of scientific and technological fields, including catalysis, solar energy conversion, thermoelectric energy conversion, bioassaying, and optoelectronic sensor devices.[1−5] As the materials approach nanosize dimensions, their physical properties change because of quantum confinement giving rise to blue-shifted optical adsorption and strong luminescence.[6] When bulk structures are perforated with well-defined arrays of pore channels, nanosized walls can be created that can exhibit electronic and optical characteristics similar to those of discrete nanodots.[7−10] Furthermore, the existence of regular porosity can enable shape-selective mass transport through the framework, which makes such systems attractive for new kinds of experimentation such as electrochemical- and photochemical-induced shape-selective molecular transformations and membrane separation development.

It is known that $[Ge_9]^{4-}$ Zintl clusters in ethylenediamine self-oxidize to form oligomers $\{[Ge_9]^{2-}\}_n^{2n-}$ $(n = 2-4)$[11,12] and linear polymer $^1/_\infty\{[Ge_9]^{2-}\}$ chains.[13] Recently, we and others described that use of group IV Zintl compounds as building units for mesoporous semiconductors.[14−16] We employed cross-linking polymerization reactions of surfactant-templated Zintl Ge^{4-} and $(Ge_9)^{4-}$ anions with Ge^{4+} to produce mesostructured germanium. These include cubic gyroidal (MSU-Ge-1) and hexagonal mesoporous (MSU-Ge-2) frameworks.[12,14] Using oxidative self-polymerization chemistry of $(Ge_9)^{4-}$ clusters, we produced a different kind of hexagonal mesoporous network (NU-Ge-1).[17] Coordinative and oxidative coupling reactions of Ge_9^{4-} with various transition-metal ions have produced interesting species, including $[Ge_9Ni(CO)]^{3-}$,[18] $[Ge_9Zn(C_6H_5)]^{3-}$,[19] $[Au_3Ge_{45}]^{9-}$,[20] and the polymeric chain

† Northwestern University.
‡ Argonne National Laboratory.

(1) Trindade, T.; O'Brien, P.; Pickett, N. L. *Chem. Mater.* **2001**, *13*, 3843–3858.
(2) Turton, R. In *The Quantum Dot*; Oxford University Press: Oxford, UK, 1995.
(3) Michalet, X.; Pinaud, F. F.; Bentolila, L. A.; Tsay, J. M.; Doose, S.; Li, J. J.; Sundaresan, G.; Wu, A. M.; Gambhir, S. S.; Weiss, S. *Science* **2005**, *307*, 538–544.
(4) (a) Ferrando, R.; Jellinek, J.; Johnston, R. L. *Chem. Rev.* **2008**, *108*, 845–910. (b) Klimov, V. I.; Ivanov, S. A.; Nanda, J.; Achermann, M.; Bezel, I.; McGuire, J. A.; Piryatinski, A. *Nature* **2007**, *447*, 441–446.
(5) (a) Dresselhaus, M. S.; Chen, G.; Tang, M. Y.; Yang, R. G.; Lee, H.; Wang, D. Z.; Ren, Z. F.; Fleurial, J.-P.; Gogna, P. *Adv. Mater.* **2007**, *19*, 1043–1053. (b) Quarez, E.; Hsu, K.-F.; Pcionek, R.; Frangis, N.; Polychroniadis, E. K.; Kanatzidis, M. G. *J. Am. Chem. Soc.* **2005**, *127*, 9177–9190.
(6) Alivisatos, A. P. *Science* **1996**, *271*, 933–937.
(7) Kanatzidis, M. G. *Adv. Mater.* **2007**, *19*, 1165–1181.
(8) Trikalitis, P. N.; Rangan, K. K.; Bakas, T.; Kanatzidis, M. G. *Nature* **2001**, *410*, 671–675.
(9) Riley, A. E.; Korlann, S. D.; Richman, E. K.; Tolbert, S. H. *Angew. Chem., Int. Ed.* **2006**, *45*, 235–241.
(10) Rangan, K. K.; Trikalitis, P. N.; Kanatzidis, M. G. *J. Am. Chem. Soc.* **2000**, *122*, 10230–10231.
(11) Xu, L.; Sevov, S. C. *J. Am. Chem. Soc.* **1999**, *121*, 9245–9246.
(12) Ugrinov, A.; Sevov, S. C. *J. Am. Chem. Soc.* **2002**, *124*, 10990–10991.
(13) Downie, C.; Tang, Z.; Guloy, A. M. *Angew. Chem., Int. Ed.* **2000**, *39*, 337–340.
(14) Armatas, G. S.; Kanatzidis, M. G. *Nature* **2006**, *441*, 1122–1125.
(15) Sun, D.; Riley, A. E.; Cadby, A. J.; Richman, E. K.; Korlann, S. D.; Tolbert, S. H. *Nature* **2006**, *441*, 1126–1130.
(16) Armatas, G. S.; Kanatzidis, M. G. *Science* **2006**, *313*, 817–820.
(17) Armatas, G. S.; Kanatzidis, M. G. *Adv. Mater.* **2008**, *20*, 546–550.
(18) Goicoechea, J. M.; Sevov, S. C. *J. Am. Chem. Soc.* **2006**, *128*, 4155–4161.
(19) Goicoechea, J. M.; Sevov, S. C. *Organometallics* **2006**, *25*, 4530–4536.
(20) Spiekermann, A.; Hoffmann, S. D.; Fässler, T. F.; Krossing, I.; Preiss, U. *Angew. Chem., Int. Ed.* **2007**, *46*, 5310–5313.

10.1021/ja802940w CCC: $40.75

$^1/_\infty\{[Hg(Ge_9)]^{2-}\}$.[21,22] These results point to the intriguing new direction where materials based on Ge_9 clusters can be anticipated using metal coordinative chemistry.

Herein, we report the general scope of the metal-linked coupling chemistry to fabricate a novel series of mesoporous binary intermetallic germanium-based materials. We present the metal-linked assembly of $(Ge_9)^{4-}$ clusters using different linking metal ions for constructing mesoporous binary compound semiconductors with hexagonal pore systems. To the best of our knowledge, this is the first time the synthesis of mesoporous intermetallic materials is demonstrated. The mesoporous structures exhibit narrow energy gaps as well as photoluminescence which depend strongly on pore wall thickness and framework composition. The photoemission spectra can be sensitive to organic molecules small enough to enter the pores and engage in electron-acceptor interactions with the semiconductor framework.

Experimental Section

Starting Materials. The K_4Ge_9 precursor was prepared according to a modified literature procedure, in inert atmosphere or under vacuum.[23] Ge and K mixed in molar ratio of 9:4.4 were heated at 900 °C for 2 d in a sealed niobium tube, enclosed in a quartz ampule under vacuum. The amphiphile *N*-eicosane-*N*,*N*-dimethyl-*N*-(2-hydroxyethyl) ammonium bromide (EDMHEAB) surfactant was prepared by reacting a stoichiometric amount of the eicosane bromide (Aldrich) with *N*,*N*-dimethylethanolamine (Aldrich) in ethanol under reflux conditions for 48 h. Pure compound was obtained by recrystallization from $CHCl_3$−ethyl acetate mixture solution.[24] The product was dried at 70 °C for 12 h and then under vacuum at room temperature for 24 h. Anhydrous ethanol and anhydrous dimethylformamide (DMF) (Aldrich) were degassed under nitrogen. Ethylenediamine (*en*) was dried over CaH_2 and then distilled from sodium/benzophenone under nitrogen and stored under nitrogen.

Synthesis of Mesoporous NU-MGe-2 (M = Sb, In, Sn, Pb, Cd). The synthesis was carried out inside the glovebox under nitrogen atmosphere. In a typical preparation, K_4Ge_9 (200 mg, 0.25mmol) dissolved in 4 mL of anhydrous *en* was stirred at room temperature, forming a clear dark red solution. In a separate flask, 0.25 mmol of $InCl_3$ or 0.50 mmol of $Pb(NO_3)_2$ and $CdCl_2$ in 1 mL formamide or 0.25 mmol of SbI_3 and SnI_4 in 1 mL anhydrous DMF form a clear solution. These solutions were added dropwise simultaneously to a clear solution of 0.9 g of EDMHEAB surfactant in 9 mL of formamide at 75−80 °C. A small precipitation of solid formed within a few seconds, and the resulting mixture was aged overnight at 80 °C under stirring. The product (EDMHEA)[MGe_9] was isolated by filtration, washed with warm (80 °C) formamide several times, and dried under vacuum at room temperature for 24 h (>80% yield).

Mesoporous solids were prepared by reacting 200 mg of (EDMHEA)[MGe_9] with 130 mg of ammonium nitrate (ion-exchange reaction) in 20 mL of anhydrous ethanol at room temperature for ∼5 min. The product was isolated by filtration, washed with anhydrous ethanol several times, and dried under vacuum at room temperature for 24 h. The ion-exchange procedure was repeated twice, and the product was heated at 80 °C under vacuum for 12 h. All manipulations were performed in inert atmosphere or under vacuum.

Absorption of Organic Molecules. Inside a glovebox, mesoporous NU-InGe-2 (10 mg) sample was dispersed in 10 mL of anhydrous chloroform containing predetermined amounts of tetracyanoethylene (TCNE) or tetrathiafulvalene (TTF). Various (at least two) aliquots of 2 mL from this suspension were placed inside 3-mm quartz tubes which were tightly shielded under nitrogen for photoluminescence experiments.

Physical Characterization. The elemental C, H, and N microanalysis was performed in a Perkin-Elmer series II CHNS/O analyzer 2400 instrument. Before the measurements, the samples were heated at 180 °C for 4 h. Thermogravimetric analysis (TGA) experiments were performed in a Shimadzu TGA-50 thermal analyzer by heating the samples to 600 °C at a heating rate of 10 °C/min under nitrogen flow of ∼20 mL/min. Powder X-ray diffraction (XRD) patterns were collected on a Rigaku ATX-G X-ray diffractometer using Ni-filtered Cu Kα (λ = 1.54098 Å) radiation (50 kV, 240 mA). Diffraction data were recorded in the 2θ range of 1−10° with a 2θ step size of 0.01° and a scanning speed of 0.1°/min. Nitrogen adsorption−desorption isotherms were measured at −196 °C on a Micromeritics ASAP 2020 sorption analyzer. Before the measurements, the samples were outgassed at 80 °C under vacuum ($<10^{-5}$ Torr) for 12 h.

The specific surface areas were calculated using the Brumauer−Emmett−Teller (BET) method[25] on the adsorption data in the relative pressure range of 0.05−0.22. The total pore volumes were estimated from the adsorbed amount at the relative pressure of P/P_o = 0.95 by applying the Gurvich rule, and the pore size distributions were obtained from the adsorption branch of the isotherms using the Barrett−Joyner−Halenda (BJH) method[26] with modified statistical film thickness equation (KJS).[27]

Transmission electron micrographs were obtained using a JSM-2100F JEOL electron microscope equipped with EDX-detector (Noran Instruments) and operated at 200 kV with a cold-field emission source. Higher angle annular dark field (HAADF) scanning transmission electron microscopy (STEM) images and energy-dispersive X-ray spectroscopy (EDS) microanalysis with probe size of 1 nm were acquired on JSM-2010F JEOL microscope. The sample was first dispersed in anhydrous ethanol and then picked up on a copper grid covered with carbon film.

X-ray photoelectron spectroscopy (XPS) was performed on an Omicron ESCA system equipped with a monochromated Al Kα X-ray (1486.6 eV) source and operated at 300 W. Samples were analyzed at pressure below 2×10^{-8} Torr with a pass energy of 25 eV and a takeoff angle of 45°. Binding energies of spectra were referred to the signature C 1s binding energy at 284.6 eV. Significant effort was made to minimize the air exposure time of the samples, which in any case was not greater than ∼2 min.

UV/vis diffuse reflectance spectra were recorded at room temperature with a Shimadzu model UV-3101PC double-beam, double monochromator spectrophotometer, using powder $BaSO_4$ as a 100% reflectance standard. Reflectance data were converted to absorption (α/S) data according to the Kubelka−Munk equation: $\alpha/S = (1 - R)^2/(2R)$, where R is the reflectance and α and S are the absorption and scattering coefficients, respectively. Photoluminescence spectra were obtained at room temperature on a Photon Technology International QM-2 spectrofluorimeter equipped with a 75 W xenon lamp and operated from 200 to 1000 nm.

Results and Discussion

Synthesis, Pore Structure, and Surface Area. The synthesis of mesoporous intermetallic germanium semiconductors was accomplished by linking $(Ge_9)^{4-}$ clusters with metal ions in the presence of appropriate cationic surfactants. Namely, the amphiphilic EDMHEAB surfactant in a mixed formamide/

(21) Nienhaus, A.; Hauptmann, R.; Fässler, T. F. *Angew. Chem., Int. Ed.* **2002**, *41*, 3213–3215.
(22) Boeddinghaus, M. B.; Hoffmann, S. D.; Fässler, T. F. *Z. Anorg. Allg. Chem.* **2007**, *633*, 2338–2341.
(23) Ugrinov, A.; Sevov, S. C. *J. Am. Chem. Soc.* **2003**, *125*, 14059–14064.
(24) Broxon, T. J.; Chung, R. P.-T. *J. Org. Chem.* **1990**, *55*, 3886–3890.
(25) Brunauer, S.; Deming, L. S.; Deming, W. S.; Teller, E. *J. Am. Chem. Soc.* **1940**, *62*, 1723–1732.
(26) Barrett, E. P.; Joyner, L. G.; Halenda, P. H. *J. Am. Chem. Soc.* **1951**, *73*, 373–380.
(27) Kruk, M.; Jaroniec, A.; Sayari, A. *J. Phys. Chem. B* **1997**, *101*, 583–589.

Table 1. Analytical Data and Chemical Compositions of As-Prepared Mesostructured and Template-Removed Mesoporous NU-MGe-2 (M = Sb, In, Sn, Pb, Cd)

material	elemental C, H, N (%)	surfactant[a] (% wt)	M/Ge_9[b]	formula
	13.83, 2.58, 1.05	17.3	1.2	$(EDMHEA)_{0.46}[Sb_{1.2}Ge_9]$
NU-SbGe-2	6.02, 1.09, 0.73	7.5		$(EDMHEA)_{0.17}[Sb_{1.2}Ge_9]$
	13.44, 2.46, 1.14	16.7	1.1	$(EDMHEA)_{0.43}[In_{1.1}Ge_9]$
NU-InGe-2	5.53, 1.11, 0.72	6.6		$(EDMHEA)_{0.15}[In_{1.1}Ge_9]$
	21.20, 3.62, 1.35	26.8	1.2	$(EDMHEA)_{0.80}[Sn_{1.2}Ge_9]$
NU-SnGe-2	5.42, 1.32, 0.73	6.4		$(EDMHEA)_{0.15}[Sn_{1.2}Ge_9]$
	15.09, 2.84, 1.10	19.1	1.8	$(EDMHEA)_{0.66}[Pb_{1.8}Ge_9]$
NU-PbGe-2	4.78, 1.01, 0.24	6.0		$(EDMHEA)_{0.18}[Pb_{1.8}Ge_9]$
	14.04, 2.63, 1.04	17.7	2.2	$(EDMHEA)_{0.53}[Cd_{2.2}Ge_9]$
NU-CdGe-2	2.90, 0.64, 0.28	3.6		$(EDMHEA)_{0.09}[Cd_{2.2}Ge_9]$

[a] Percent of surfactant content on the basis of elemental C, H, N, and TGA data. [b] EDS elemental data normalized to nine-atom Ge cluster.

ethylenediamine solution was found to be excellent in templating the organized cross-linking polymerization of deltahedral $(Ge_9)^{4-}$ clusters by various metal ions (eq 1).

$$EDMHEAB + (Ge_9)^{4-} + (4/n)M^{n+} \rightarrow (EDMHEA)_x[M_{4/n}Ge_9] \quad (1)$$

where M = In, Sb, Sn, Pb, and Cd.

The idea behind this reaction was to build an extended M/Ge_9 network by coordinatively interlinking the germanium clusters with metal ions through M−Ge bonding. Removal of the surfactant from the framework by ion exchange with NH_4NO_3 in ethanol followed by mild heating (80 °C) under vacuum to evolve NH_3 gave the mesoporous materials NU-MGe-2 (eq 2).

$$(EDMHEA)_x[M_{4/n}Ge_9] + NH_4^+ \rightarrow (NH_4^+)_x[M_{4/n}Ge_9] \rightarrow H_xM_{4/n}Ge_9 + NH_3 \quad \text{(NU-MGe-2)} \quad (2)$$

The framework surface of these mesoporous materials is H-passivated via Ge−H_x bonds according to the infrared spectroscopy (Supporting Information).

The chemical composition of as-prepared mesostructured and mesoporous NU-MGe-2 was determined with EDS, elemental C, H, N, and TGA analysis. Analytical data and the estimated chemical formulas for the NU-MGe-2 samples are given in Table 1. Elemental EDS microanalysis of the inorganic frameworks indicated the expected atomic ratio between the linking metal and Ge_9 cluster; that is, ∼1 for Sb^{3+}, In^{3+}, and Sn^{4+} and close to 2 for Pb^{2+} and Cd^{2+} ions, in agreement with eq 1 (Table 1). The EDS spectra showed only signals from the expected elements (i.e., M and Ge). They showed the absence of any traces of potassium or halides, suggesting complete metathesis and cross-linking polymerization of $(Ge_9)^{4-}$ clusters by metal ions.

The elemental C, H, N, and TGA results of the mesoporous products indicated only a ∼6−7% of surfactant remaining in the pores after the template-removal procedure (Table 1). Further efforts to eliminate completely the surfactant molecules from the pores by repeating the ion-exchange procedure decreased the surfactant content to as low as ∼2%, but caused significant degradation of the pore order.

Figure 1 shows powder XRD patterns of as-prepared and mesoporous NU-MGe-2. All mesostructures show a relatively broad but well-defined diffraction peak at low scattering angles (1−3°), indicating mesoscopic order. Upon template removal, the main diffraction peaks broaden and shift to a slightly higher scattering angle, indicating a small contraction of the pore spacing. The broadening of the main diffraction peaks suggests

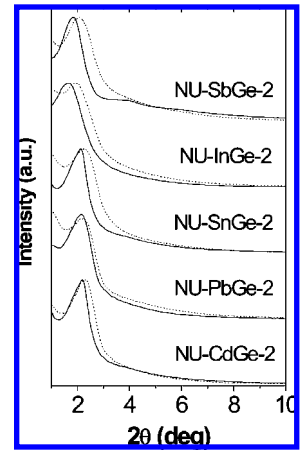

Figure 1. Low-angle XRD patterns of as-prepared containing surfactant (solid) and template-removed mesoporous (dashed lines) NU-MGe-2 (M = Sb, In, Sn, Pb, Cd) materials.

a decrease in the coherent domain size upon surfactant removal. The lack of Bragg diffraction peaks at high angles (>10°) signifies the nonperiodic nature of the inorganic framework.

Direct evidence of the pore organization was obtained with transmission electron microscopy (TEM). Figure 2 displays typical TEM images and the corresponding fast Fourier transforms obtained from mesoporous NU-MGe-2. The TEM images show discernible domains of hexagonal arrays of cylindrical pore channels, revealing *p6mm* pore symmetry analogous to that of MCM-41.[28] On the basis of the XRD patterns and TEM analysis, the lattice constants (a_0) of hexagonal motif, estimated from the *d*-spacing ($a_0 = 2/\sqrt{3}d_{100}$) of the first (100) diffraction peak, are shown in Table 2.

To determine whether the linking metal atoms are located within the framework and not aggregated as a separated phase, we acquired HAADF images on the mesoporous samples using high-resolution STEM. The elemental composition of the local structure was determined by STEM X-ray microanalysis. Figure 3 shows typical HAADF STEM images of mesoporous NU-SbGe-2 and NU-PbGe-2. The HAADF images depict a parallel array of cylindrical pore channels where the high density region of wall structure appears as discrete white lines and the empty pores as dark spaces. The EDS line spectra acquired across the thin area of the framework, shown in Figure 3, indicate atomic ratio Sb/Ge_9 ≈ 1.1 and atomic ratio Pb/Ge_9 ≈ 1.8 for mesoporous NU-SbGe-2 and NU-PbGe-2, respectively, which is consistent with the nominal bimetallic composition.

Nitrogen sorption experiments were performed to probe the permanent mesoporosity of the title materials. Figure 4 shows the nitrogen adsorption−desorption isotherms of several mesoporous NU-MGe-2 semiconductors. All adsorption branches exhibit typical type IV curves according to the IUPAC classification, with a distinct step at relative pressure (P/P_o) ≈ 0.16 that is attributed to nitrogen condensation in uniform mesopores. A rapid increase in the adsorption curve at high relative pressure (P/P_o > 0.9) was observed, implying the presence of voids between the particles.

The title mesoporous materials were found to have BET surface areas in the range 127−277 m^2/g and total pore volumes in the range 0.15−0.26 cm^3/g. These surface areas are very high if we account for their heavier framework wall structure. For

(28) Kresge, C. T.; Leonowicz, M. E.; Roth, W. J.; Vartuli, J. C.; Beck, J. S. *Nature* **1992**, *359*, 710–712.

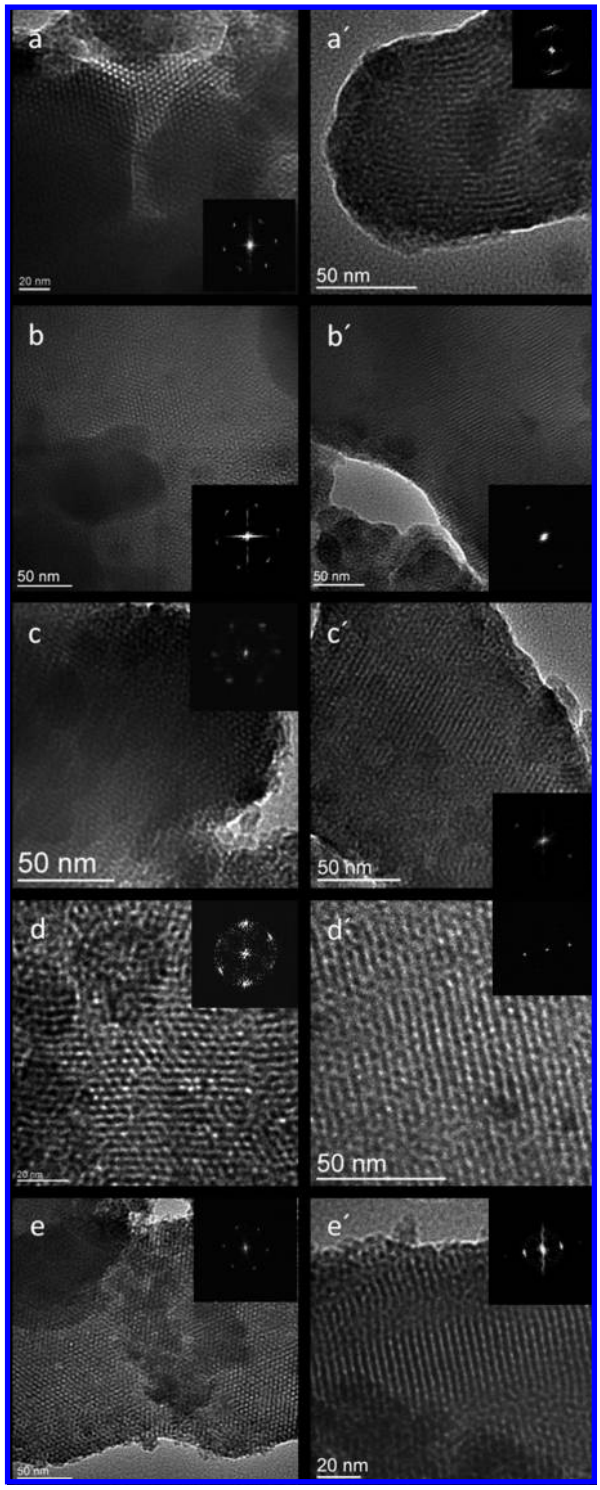

Figure 2. TEM images of mesoporous (a and a′) NU-SbGe-2, (b and b′) NU-InGe-2, (c and c′) NU-SnGe-2, (d and d′) NU-PbGe-2, and (e and e′) NU-CdGe-2 samples viewed along the pore channel axis (left) and perpendicular to the channel axis (right). The corresponding fast Fourier transform images are shown in the insets.

comparison purposes, these values correspond, respectively, to silica equivalent surface areas of 403−858 m^2/g. All the textural properties of the NU-MGe-2 family are given in Table 2. Analysis of the adsorption branches using the modified BJH method reveals a narrow distribution of pore sizes, as indicated from the full width of the half-maximum (fwhm) of the peaks, with the peak maximum being in the 2.7−2.8 nm range. The very similar pore size of the NU-MGe-2 samples indicates good replication of the inorganic structures around the surfactant template. The pore-to-pore distance obtained from the XRD data together with the pore size obtained from the BJH method indicate a framework wall thickness of ∼2 nm for NU-MGe-2 (M = Sb, In, Sn, and Cd) and ∼2.4 nm for NU-PbGe-2. The small increase in wall thickness for NU-PbGe-2 could be attributed to the larger radius of the incorporated Pb atoms.

Table 2. Textural Parameters of Mesoporous NU-MGe-2 (M = Sb, In, Sn, Pb, Cd) Materials

mesoporous	surface area[a] (m^2/g)	pore volume[b] (cm^3/g)	pore size (nm)	fwhm[c] (nm)	a_0 (a_0[d]) (nm)	wall thickness[e] (nm)
NU-SbGe-2	277 (858)	0.25	2.8	1.1	4.5 (4.7)	1.7
NU-InGe-2	223 (680)	0.26	2.7	1.2	4.6 (4.7)	1.9
NU-SnGe-2	215 (663)	0.15	2.7	1.1	4.5 (4.8)	1.8
NU-PbGe-2	171 (642)	0.18	2.8	1.2	5.2 (6.1)	2.4
NU-CdGe-2	127 (403)	0.20	2.8	0.7	4.8 (5.5)	2.0

[a] Equivalent surface area based on molecular weight calculations and assuming the equivalent triatomic "M_xGe_{3-x}" unit structure, analogous to SiO_2 formula. [b] Cumulative pore volume at (P/P_o) equal to 0.95. [c] Full-width of the half-maximum of psd. [d] Unit cell constant of as-prepared material. [e] Framework wall thickness WT = $a_0 - d$, where d is the size of the pores.

Spectroscopy. The oxidation state of Ge atoms and linking metal atoms in the mesoporous framework was examined with XPS. Generally, the binding energy of an atom increases as the oxidation state increases.[29] The XPS spectra reveal single Ge 3d core-level signals with binding energy between 29.2 and 29.5 eV, which is very close to the reported Ge 3d binding energy of zerovalent Ge (29.0 eV)[30] (Supporting Information). This is much lower that the binding energy of the Ge 3d peak for GeO_2 of 32.5 eV.[31] The slight shift in binding energies to higher values (0.2−0.5 eV) could indicate that some Ge atoms are in partially oxidized form. Similarly, the XPS spectra of the linking metal atoms imply Sb $3d_{5/2}$, In $3d_{5/2}$, Sn $3d_{5/2}$, Pb $4f_{7/2}$, and Cd $3d_{5/2}$ core level signals with binding energies very close to those observed for zerovalent elements[32] (Figure 5 and Supporting Information). All the core-level binding energies of germanium and metal-linking atoms are listed in Table 3.

The XPS data suggest that the Ge and linking metal atoms in the framework structure are in relative low oxidation state. This is in line with expectations for an MGe_9 composition of these materials. Similar electronic configuration was found in metal−alloy Ge-containing phases consisting of interconnected metal atoms.[33]

The electronic absorption spectra of mesoporous NU-MGe-2 show sharp optical absorption onsets associated with band gap transitions in the energy range 1.48−1.70 eV (Figure 6). The energy gap in these materials is significantly blue-shifted (∼1 eV hypsochromic shift) compared to that of bulk Ge (0.66 eV) and varies with the linking metal ion in the order $Sb^{3+} \approx In^{3+}$

(29) Kibel, M. H. X-ray Photoelectron Spectroscopy. In *Surface Analysis Methods in Materials Science*, 2nd ed.; O'Connor, D. J., Sexton, B. A., Smart, R. St. C., Eds.; Springer: Berlin, 2003; Chapter 7, pp 175−201.
(30) Lu, X.; Korgel, B. A.; Johnston, K. P. *Chem. Mater.* **2005**, *17*, 6479–6485.
(31) Hollinger, G.; Kumurdjian, P.; Mackowski, J. M.; Pertosa, P.; Porte, L.; Duc, T. M. *J. Electron Spectrosc. Relat. Phenom.* **1974**, *5*, 237–245.
(32) *Handbook of X-ray Photoelectron Spectroscopy: A Reference Book of Standard Spectra for Identification and Interpretation of XPS Data*; Chastain, J., King, R. C., Jr., Eds.; Physical Electronics: Eden Prairie, MN, 1995.
(33) Guloy, A. M.; Corbett, J. D. *Inorg. Chem.* **1996**, *35*, 4669–4675.

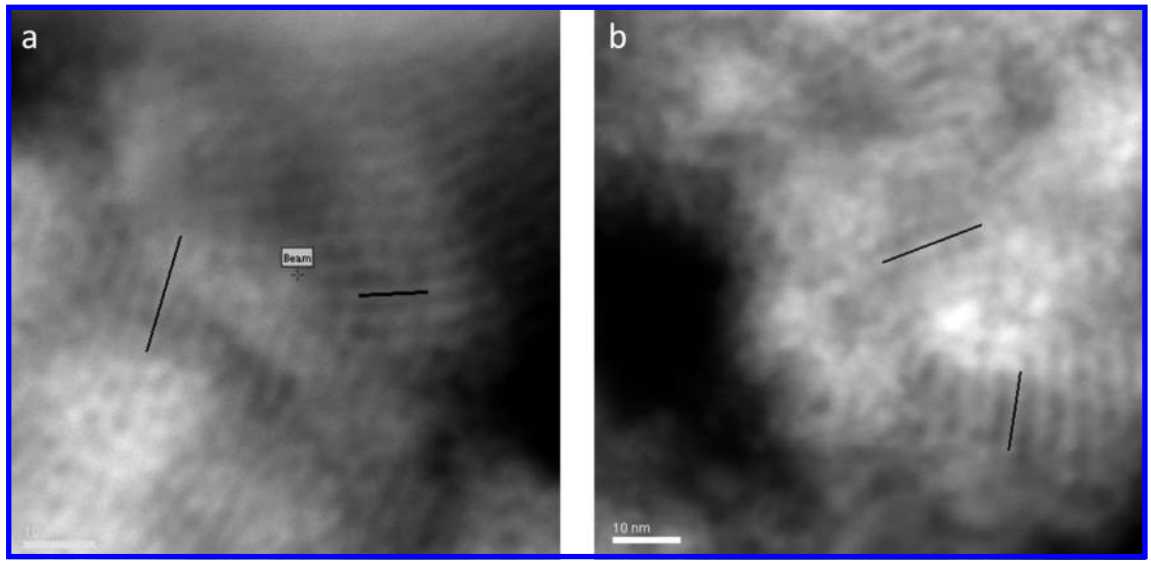

Figure 3. High-resolution HAADF STEM images of mesoporous (a) NU-SbGe-2 and (b) NU-PbGe-2 materials looking perpendicular to the pore channel axis. The framework wall structure appeared as discrete white lines, and the empty pores appeared as dark spaces. The black lines and the spot indicate the areas where the EDS line analysis data was acquired.

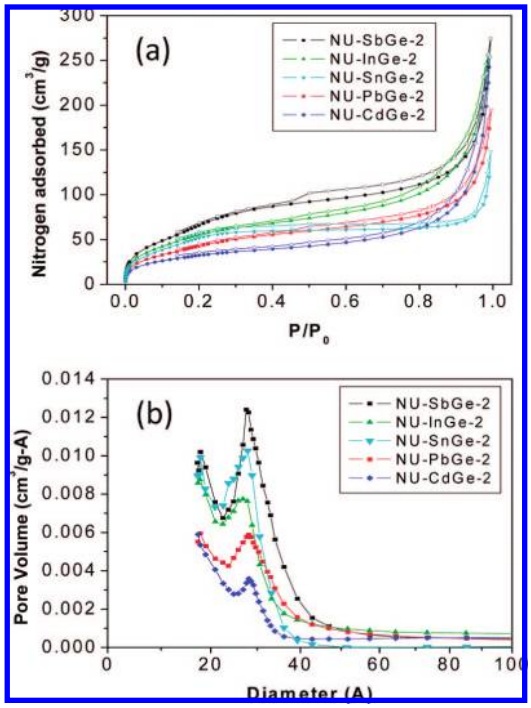

Figure 4. (a) Nitrogen adsorption−desorption isotherms at −196 °C of mesoporous NU-MGe-2 (M = Sb, In, Sn, Pb, Cd) and (b) BJH pore size distributions calculated from the adsorption branches.

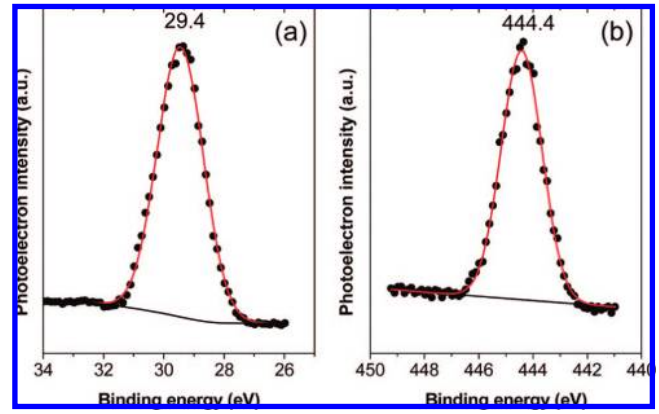

Figure 5. Typical high-resolution (a) Ge 3d and (b) In $3d_{5/2}$ core-level photoelectron spectra of mesoporous NU-InGe-2.

> Sn^{4+} > Cd^{2+} > Pb^{2+} (Table 3). The systematic variation with metal ion also supports the fact that the linking metal atoms are an integral part of the framework and their orbitals participate in defining its electronic structure. The mesoporous forms have a slightly wider energy gap than the as-prepared materials (20−30 meV), reflecting the slightly different pore structure and/or possible slight oxidation (inadvertent) of inorganic framework after template removal (Figure S6).

The considerable blue shift in energy gap in going from bulk elemental Ge to the mesoporous MGe_9 frameworks is similar to those observed in pure mesoporous germanium,[21,22] and it is due to the substantial dimensional reduction of the framework wall thickness (∼2 nm) in NU-MGe-2. This is reminiscent of the quantum-confinement-induced increase in energy gap observed in nanosized semiconductors.[34−37]

Whereas bulk Ge in not a luminescence solid, the mesoporous structures of NU-MGe-2 exhibited strong light emission at room temperature when excited with photons with energy above the bang gap (Figure 7). The peak maximum of the photoluminescence (PL) spectrum varied from 740 to 845 nm, depending on the chemical composition of the framework (Table 3). The PL emission of these materials is observed very near the band-edge adsorption, suggesting a band-to-band-type luminescence and minimal quenching effect of trap states or surface defects to the emission process. Generally, such a band-edge emission is associated with recombination of electron−hole carriers in quantized energy states between the higher valence and lower

(34) Nakamura, Y.; Watanabe, K.; Fukuzawa, Y.; Ichikawa, M. *Appl. Phys. Lett.* **2005**, *87*, 1–3.
(35) Lu, X.; Ziegler, K. J.; Ghezelbash, A.; Johnston, K. P.; Korgel, B. A. *Nano Lett.* **2004**, *4*, 969–974.
(36) Taylor, B. R.; Kauzlarich, S. M.; Lee, H. W. H.; Delgado, G. R. *Chem. Mater.* **1998**, *10*, 22–24.
(37) Yang, H.; Yao, X.; Wang, X.; Xie, S.; Fang, Y.; Liu, S.; Gu, X. *J. Phys. Chem. B* **2003**, *107*, 13319–13322.

Table 3. Summary of Photoelectron Binding Energies, Energy Band Gaps, and Peaks of Photoluminescence Signals for the Mesoporous NU-MGe-2 (M = Sb, In, Sn, Pb, and Cd) Materials

			PL peaks/eV (nm)	
mesoporous	XPS binding energies (eV)	band gap[a] (eV)	excitation	emission
NU-SbGe-2	29.4 (Ge_{3d}), 121.5 ($Ge_{2p3/2}$), 527.8 ($Sb_{3d5/2}$), 537.3 ($Sb_{3d3/2}$)	1.70 (1.67)	1.83 (680)	1.65 (750)
NU-InGe-2	29.4 (Ge_{3d}), 444.4 ($In_{3d5/2}$)	1.68 (1.66)	2.43 (510)	1.68 (740)
NU-SnGe-2	29.3 (Ge_{3d}), 485.1 ($Sn_{3d5/2}$), 493.5 ($Sn_{3d3/2}$)	1.65 (1.62)	1.77 (700)	1.63 (760)
NU-PbGe-2	29.2 (Ge_{3d}), 18.1 (Pb_{5d}), 137.2 ($Pb_{4f7/2}$), 141.5 ($Pb_{4f5/2}$)	1.48 (1.46)	1.60 (775)	1.47 (845)
NU-CdGe-2	29.5 (Ge_{3d}), 404.8 ($Cd_{3d5/2}$)	1.62 (1.59)	1.79 (695)	1.62 (775)

[a] The energy band gap of as-prepared surfactant containing material is given in parentheses.

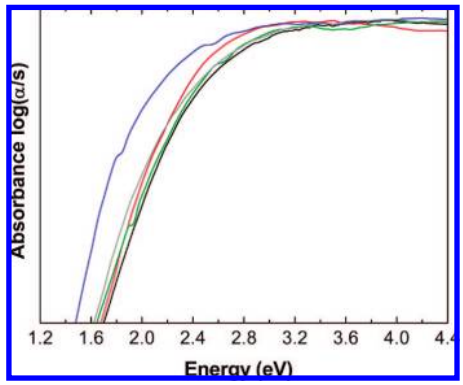

Figure 6. Optical absorption spectra of mesoporous metal−germanium semiconductors: NU-SbGe-2 (black), NU-InGe-2 (red), NU-SnGe-2 (green), NU-PbGe-2 (blue), and NU-CdGe-2 (gray lines).

conduction band. Since the surfactant molecules are not photoluminescent, the chemically tunable emission peak in the NU-MGe-2 materials implies that the emission response is an intrinsic property of the inorganic framework. This is a remarkable property when we consider that these porous frameworks are in fact amorphous and typically such random structures show poor emission properties at room temperature.

Partial oxidation of the inorganic framework by exposure in air altered the PL excitation and emission properties of the materials. For example, an air-oxidized sample of NU-InGe-2 exhibited less intense and more blue-shifted PL excitation and emission spectra at ~480 and ~730 nm, respectively, compared to the pristine NU-InGe-2 analogue (Figure 7).

An interesting feature of the PL response is that it can be significantly altered by incorporating organic molecules with electron-transfer properties. We examined the ability of mesoporous NU-InGe-2 to change its PL emission signal upon treatment with the electron-acceptor TCNE and the electron-donor TTF molecules in chloroform. The incorporation of TCNE and TTF organic molecules into the pore structure of NU-InGe-2 was confirmed by infrared spectroscopy (Figure S7). The NU-InGe-2 exhibited significant changes in the intensity of the PL emission signal by adsorbing different amounts of TCNE under the excitation line of 510 nm (Figure 8). The photoemission intensity of TCNE@NU-InGe-2 decreased continuously with increasing TCNE concentration (Figure 8b).

Compared to PL observed from Ge nanocrystals, the emission energies in NU-MGe-2 are much lower. The nanocrystals show visible photoluminescence properties that are associated with the surface.[38] It has been shown that excitons in this case are localized near the surface region and the strong coupling of localized excitons and local stretch vibrations of surface species cause fine structures in the PL spectrum. It is possible that similar phenomena are at play in the NU-MGe-2, and any created exciton must be near the surface given that the walls are only 1.5−2-nm thick (Table 2). The structure observed in several PL spectra of the mesoporous compounds in Figure 7b is consistent with this interpretation.

Interestingly, although the electron-donor TTF molecules do enter the mesoporous NU-InGe-2 framework, they did not affect its PL excitation and emission properties (Figure S8). This observation clearly indicates that the electronic structure of NU-InGe-2 semiconductor is active, selective, and sensitive toward organic molecules with electron-acceptor properties. In Scheme 1, we propose a possible model to explain the observed behavior and to link the electron-transfer properties of guest molecules with the PL emission of NU-InGe-2 semiconductor. The quenching properties of TCNE suggest that its lowest unoccupied molecular orbital (LUMO) lies at comparable or lower energy than the bottom of the conduction band of NU-InGe-2. In this case, electrons from the conduction band of the NU-InGe-2 relax rapidly to the empty LUMO of TCNE with subsequent nonradiative electron transfer to the valence band (HOMO) of NU-InGe-2. Correspondingly, the lack of quenching ability of TTF would suggest that its LUMO lies higher in

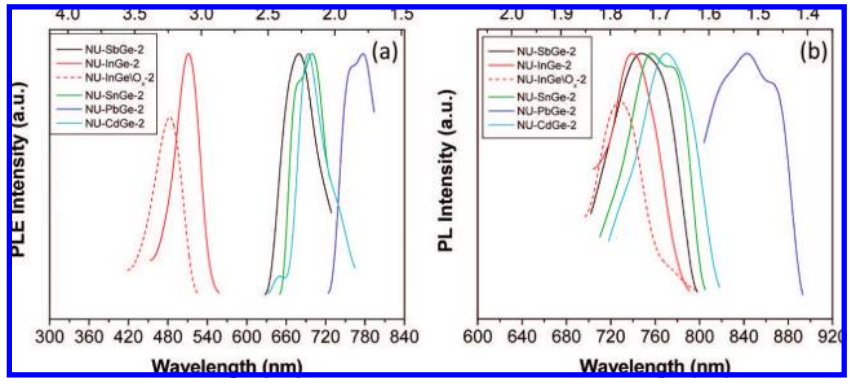

Figure 7. Photoluminescence (a) excitation and (b) emission spectra of mesoporous NU-MGe-2 (M = Sb, In, Sn, Pb, Cd) semiconductors at room temperature. The relative PL excitation and emission spectra of oxidized NU-InGe-2 (dashed line) upon air exposure for ~15 min are also given.

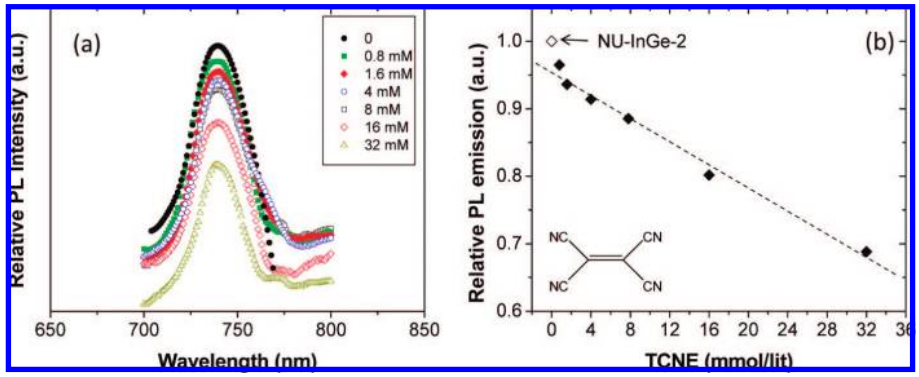

Figure 8. (a) Relative PL emission spectra of mesoporous NU-InGe-2 and TCNE@NU-InGe-2 semiconductors as a function of the TCNE concentration and (b) the TCNE concentration dependence of the PL emission peak of mesoporous NU-InGe-2. The straight line fitting the data is given as a guide to the eye ($R^2 = 0.9938$).

Scheme 1. Schematic Diagram Showing Possible Energetic Interactions between the Electronic Band Structure of NU-InGe-2 and the Frontier Molecular Orbitals of TCNE and TTF

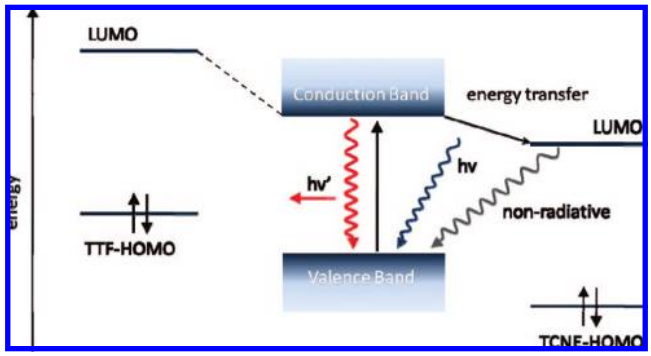

energy than the conduction band minimum, and therefore, no energy transfer is possible.

The results imply that these materials can comprise active components in light emitting sensors and optoelectronic devices. Additional work, however, is required to better assess and understand the PL response of these materials against a variety of donor and acceptor species and lifetime of the excitation/de-excitation process.

Conclusions

The hexagonal mesoporous metal−germanium-based semiconductors NU-MGe-2 (M = Sb, In, Sn, Pb, and Cd) are stable and possess a regular array of pore channels that result in large surface areas. The materials display wall thickness-dependent optical absorption properties. The absorption edge shifts hypsochromically with decreasing thickness of the framework wall, a trend that is similar to that in quantum dots. The electronic structure of the framework can be modulated by the metal ion which is reflected in a corresponding dependence of the energy gap. The mesoporous structures of NU-MGe-2 are strongly luminescent at room temperature when excited above the band gap with a peak maximum depending of the chemical composition of the framework. The light emission occurs at wavelengths near the band-edge adsorption, suggesting a band-to-band-type luminescence and negligible quenching effect of trap states or surface defects to the emission process. This suggests possible application in visible light photocatalysis and solar energy conversion. Since the NU-MGe-2 is mostly surface, the photoemission intensity can be quenched when interacting with electron-acceptor molecules entering the structure, making these materials promising for investigations of shape-selective energy-transfer donor−acceptor interactions.

Acknowledgment. Financial support from the Nanoscale Science and Engineering Initiative of the National Science Foundation under NSF Award Number EEC-0647560 is gratefully acknowledged. This work made use of the Electron Probe Instrumentation Center (EPIC) and Keck Interdisciplinary Surface Science (Keck-II) facility of NUANCE Center at Northwestern University.

Supporting Information Available: TGA profiles of as-prepared and mesoporous NU-MGe-2, XPS spectra of mesoporous samples, FTIR spectra of mesoporous NU-InGe-2 and hybrids TCNE@NU-InGe-2 and TTF@NU-InGe-2, and PL excitation and emission spectra of hybrid TTF@NU-InGe-2. This material is available free of charge via the Internet at http://pubs.acs.org.

JA802940W

(38) Okamoto, S.; Kanemitsu, Y. *Phys. Rev. B* **1996**, *54*, 16421–16424.